



CHORUS

This is the accepted manuscript made available via CHORUS. The article has been published as:

Vibrational properties of quasi-two-dimensional colloidal glasses with varying interparticle attraction

Matthew D. Gratale, Xiaoguang Ma, Zoey S. Davidson, Tim Still, Piotr Habdas, and A. G. Yodh

Phys. Rev. E **94**, 042606 — Published 20 October 2016

DOI: [10.1103/PhysRevE.94.042606](https://doi.org/10.1103/PhysRevE.94.042606)

1 **Vibrational properties of quasi-2D colloidal glasses with varying**
 2 **interparticle attraction**

3 Matthew D. Gratale,^{1,*} Xiaoguang Ma,^{1,2,*} Zoey S.

4 Davidson,¹ Tim Still,¹ Piotr Habdas,^{3,†} and A. G. Yodh^{1,†}

5 *¹Department of Physics and Astronomy,*

6 *University of Pennsylvania, Philadelphia, PA 19104, USA*

7 *²Complex Assemblies of Soft Matter, CNRS-Solvay-UPenn UMI 3254,*

8 *Bristol, Pennsylvania 19007-3624, USA*

9 *³Department of Physics, Saint Joseph's University, Philadelphia, PA 19131, USA*

10 (Dated: September 22, 2016)

Abstract

We measure the vibrational modes and particle dynamics of quasi-2D colloidal glasses as a function of interparticle interaction strength. The interparticle attractions are controlled via a temperature-tunable depletion interaction. Specifically, the interparticle attraction energy is increased gradually from a very small value (nearly hard-sphere) to moderate strength ($\sim 4k_B T$), and the variation of colloidal particle dynamics and vibrations are concurrently probed. The particle dynamics slow monotonically with increasing attraction strength and the particle motions saturate for strengths greater than $\sim 2k_B T$, *i.e.*, as the system evolves from a nearly repulsive glass to an attractive glass. The shape of the phonon density of states are revealed to change with increasing attraction strength, and the number of low-frequency modes exhibits a cross-over for glasses with weak compared to strong interparticle attraction at a threshold of $\sim 2k_B T$. This variation in the properties of the low frequency vibrational modes suggests a new means for distinguishing between repulsive and attractive glass states.

* both authors contributed equally to this work

† corresponding author

11 I. INTRODUCTION

12 Many properties of glasses depend on the interactions between constituent particles [1–
13 25]. In colloidal glasses with high packing fraction, for example, two qualitatively different
14 states have been observed that depend on the strength of the short-range attraction between
15 particles [9–19]. Glasses with weak interparticle attraction reside in a so-called “repulsive”
16 glass state, and glasses whose constituents experience strong interparticle attraction reside
17 in an “attractive” glass state. The existence of these two states has been confirmed by
18 experiment [10–13, 15, 19] and simulation [3, 9, 20, 21], and the constituent particle dynamics
19 in repulsive versus attractive glasses have also been observed to be different [9–15]. Most
20 previous studies, however, tend to compare these properties in two extreme limits, *e.g.*,
21 hard-sphere glasses versus glasses with very strong interparticle attraction. Indeed, to our
22 knowledge, few studies have explored the cross-over behavior of colloidal glasses as the
23 interparticle attraction strength is gradually increased from nearly hard-sphere to strongly
24 attractive.

25 The differences in properties between glassy states arise from different mechanisms of
26 dynamical arrest. In repulsive glasses, the particle dynamics slow down due to local crowd-
27 ing. Particles are trapped in entropic “cages” created by neighboring particles. By contrast,
28 in attractive glasses, in addition to local crowding, the particle dynamics are slowed even
29 more as a result of strong interparticle attractions. Further, the heterogeneous dynamics of
30 attractive glasses occurs over a larger range of length and time scales compared to repul-
31 sive glasses [15], and the cooperative rearrangement regions (CRRs) in repulsive glasses are
32 string-like, while in attractive glasses CRRs are compact [15]. These differences in dynami-
33 cal arrest mechanism also lead to variation of bulk rheological properties, for example, the
34 phenomenon of two-step yielding in attractive glasses [23].

35 Theory supports some of these observations. Mode coupling theory (MCT) predicts that
36 densely packed glasses with short-range interparticle attraction have two distinct arrested
37 states [1, 6, 16–18]. MCT also predicts behavior at the cross-over between repulsive and
38 attractive glass states. In particular, the transition predicted by MCT [1, 6, 16–18] is
39 characterized by discontinuous jumps in various quantities with respect to an attractive
40 potential minimum. The Debye-Waller factor, or the non-ergodicity parameter, for example,
41 is a transition indicator and was found to exhibit a jump as a function of reduced temperature

42 $k_B T/u_0$, where u_0 is the depth of the interparticle potential well, *i.e.*, the attraction strength
43 [17].

44 In this contribution we investigate the phonon modes and particle dynamics of glasses
45 in the transition region. In general, disordered solids such as glasses show an excess of
46 low-frequency vibrational modes. This excess is not predicted by the Debye model of simple
47 crystals and is known as the “boson” peak [26]. The boson peak is commonly exhibited at low
48 frequencies by a plot of the vibrational Density of States ($DOS(\omega)$) scaled by the expected
49 Debye behavior, *i.e.*, $DOS(\omega)/\omega^{d-1}$, where d is the sample dimension. The presence and
50 height of the boson peak is used as an indicator of the glass transition [27–32]. Experiment
51 and simulation have also found that these low-frequency modes are quasi-localized and
52 display enhanced participation in regions prone to rearrangements [27, 33–46].

53 Previously, the behavior of the vibrational $DOS(\omega)$ was shown to vary when crossing
54 from an attractive glass state to the gel state [22]; in this case, traditional order parameters
55 did not prove useful for characterizing the transition. Note, however, this previous work
56 studied vibrational phonons in disordered materials as a function of packing fraction with a
57 constant, strong interparticle attraction. It was observed that sparsely packed gel-like states
58 have an excess of low frequency modes compared to densely packed attractive glass states.
59 The excess of modes, in this case, arose largely from localized vibrations involving small
60 clusters of particles. Stimulated by these findings, and previous work on glasses, the present
61 contribution explores how the character of vibrational modes changes in the transition region
62 between repulsive and attractive glasses at constant packing fraction.

63 To this end, we vary the interparticle attraction strength between colloidal particles con-
64 fined in quasi-2D sample cells using temperature-tunable depletant micelles [47, 48]. The
65 vibrational properties of the glass are measured as a function of temperature, at approx-
66 imately constant packing fraction, as the system evolves from a nearly hard-sphere glass
67 to an attractive glass. Our expectation is that vibrational signatures will distinguish the
68 two glassy regimes, and indeed we observe evidence of a cross-over transition from the re-
69 pulsive glass to the attractive glass at an interparticle attraction strength of approximately
70 $2k_B T$. As the interparticle attraction is increased through this regime, the $DOS(\omega)$ of the
71 system at low frequencies decreases and saturates for attractions strengths greater than
72 $\sim 2k_B T$. Moreover, these low frequency modes exhibit a quasi-localized character for at-
73 tractions below $\sim 2k_B T$ and a more extended character for attractions above $\sim 2k_B T$. The

74 observations suggest that the variations of the vibrational $DOS(\omega)$ could serve as an indica-
75 tor of repulsive-to-attractive transitions associated with colloidal glasses. The experimental
76 results should stimulate new theoretical and simulation investigation of vibrations in glasses
77 and, in combination, experiment and theory could provide further insight into these systems.

78 II. EXPERIMENTAL METHODS

79 Samples solutions of silica spheres with diameters $1.2 \mu\text{m}$ (Bangs Laboratories) and
80 $1.57 \mu\text{m}$ (Thermo Scientific) are prepared with a 1 : 1 number ratio. The polydispersity
81 estimated by the manufacturer is 10-15% for the small particles and is 2.5% for the large
82 particles. When the spheres are densely packed, the size ratio (≈ 1.3) and number ratio
83 help frustrate crystallization [49–51], and thus can be used to create geometrically disordered
84 colloidal glasses. The particles reside in a solution containing 44 mM hexaethylene glycol
85 monododecyl ether (C_{12}E_6) surfactant micelles and 17 mM NaCl in water. The negatively
86 charged silica spheres in water are well approximated as hard-spheres due to the strong
87 screening by the added salt. The use of C_{12}E_6 micelles as depletants provides a temperature
88 tunable depletion interaction; wherein the strength of the interparticle attraction increases
89 as sample temperature is increased due to the changing length distribution of the rod-like
90 micelles [48].

91 We use wedge cells in this experiment to create large quasi-2D domains ($> 8 \text{ mm}^2$ in
92 area) of densely packed colloidal suspension. The construction of the wedge cells is adapted
93 from the procedure by Gerbode *et al* [52]. The angle of the wedge $\approx 8 \times 10^{-4}$ degrees is
94 shallow enough so that over the field of view ($60 \mu\text{m}$ by $60 \mu\text{m}$) the cell walls are effectively
95 parallel. We first inject $5 \mu\text{L}$ of sample solution with a volume fraction of approximately
96 0.1 into the wedge cell using a pipette. Then we seal the cells peripherally with optical glue
97 (Norland 65) cured for 30 minutes under a UV lamp. The completed sample cells are placed
98 vertically on the bench with the wedge pointing down for two days. Silica spheres sediment
99 to the wedge side and form large domains of densely packed colloidal glass with a packing
100 fraction $\phi = 0.82$.

101 The sample cell is placed on the stage of an inverted microscope (Zeiss Axiovert 135) and
102 viewed from below using bright field microscopy. With a $100\times$ oil immersion objective and
103 a $2.5\times$ internal magnifier, $N_{tot} \approx 1700$ particles are in the field of view. Videos of particle

104 motion are recorded at 100 frames per second for 100,000 frames using a monochrome CMOS
 105 camera (EoSens1362, Mikrotron). Commercial image acquisition software (XCAP, EPIX) is
 106 used to control the camera and stream video frames to the hard drive of a host computer.
 107 Particle trajectories are obtained from the video using standard particle-tracking algorithms
 108 [53] with an accuracy of ~ 10 nm in particle positions. Videos were taken at 12 sample
 109 temperatures ranging from 23 °C to 35 °C with 1 °C increments obtained using an objective
 110 heater (Bioprotechs).

111 We calculate vibrational modes of the colloidal samples from particle trajectories [27,
 112 28, 54]. To this end, we follow the procedure originally suggested with some corrections
 113 developed later that improve upon these procedures; all of these techniques and corrections
 114 are described in detail in previous work [22, 27, 28, 54–62]. Briefly, we first calculate the time-
 115 averaged covariance matrix $\langle C_{ij} = u_i(t)u_j(t) \rangle_t$, where $u_i(t)$ are particle displacements from
 116 their average positions. In the harmonic approximation, the covariance matrix is directly
 117 related to the matrix of effective spring constants, K , connecting particles in an undamped
 118 shadow system, *i.e.*, by $(C^{-1})_{ij}k_B T = K_{ij}$. D is the dynamical matrix of this shadow system
 119 and is related to K by $D_{ij} = K_{ij}/m_{ij}$, where $m_{ij} = \sqrt{m_i m_j}$ is the reduced mass and m_i is
 120 the mass of particle i . From the eigenvalues of the dynamical matrix the squared frequencies
 121 of vibrational modes of the system, ω^2 , can be calculated. The corresponding eigenvector,
 122 $\vec{e}_i(\omega)$, represents the displacement amplitudes of the given vibrational mode at frequency ω
 123 for the particle i .

124 III. RESULTS AND DISCUSSION

125 A. Pair correlation functions

126 We measure the sample pair correlation function, $g(r)$, at different temperatures. This
 127 measurement enables us to ascertain radial structure variation as a function of attraction
 128 strength. In Figure 1 we show measured $g(r)$'s at six temperatures. The results exhibit
 129 structural features commonly observed in bidisperse dense colloidal suspensions. Specifically,
 130 three peaks are observed near the first shell of immediate neighbors; these peaks are due
 131 to small-small, small-large, and large-large particle separations, respectively. The broad
 132 shoulder of the first peak is due in part to the large polydispersity (10-15%) of the small

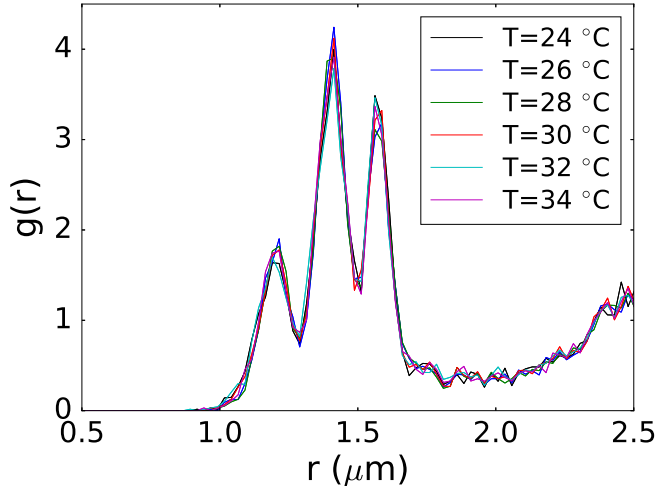


FIG. 1. Pair correlation function, $g(r)$, for a representative subset of temperatures (24 °C, 26 °C, 28 °C, 30 °C, 32 °C, and 34 °C).

133 particles; on the other hand, the third peak due to the contacts between large particles has
 134 a much narrower shoulder due to the uniformity of the large particles. The measured $g(r)$'s
 135 show little change as the strength of interparticle attraction increases. Thus, measurements
 136 of pair correlation functions do not appear to capture any feature that reveals a cross-over
 137 transition from repulsive glass to attractive glass (*i.e.*, within our signal-to-noise); note, small
 138 structure changes in the radial functions have been discerned in other systems [11, 13].
 139 At high packing fractions the pair correlation function generally depends on the particle
 140 interaction at very short range, and, within our experimental resolution, this short-range
 141 repulsive part of the interparticle potential is similar for particles in both the repulsive and
 142 attractive glasses. This observation is consistent with the classic work of Weeks, Chandler
 143 and Andersen [63], and recent computer simulation results [5, 64]. Absent obvious structural
 144 effects, we shift to explore dynamic features to characterize the transition, including mean-
 145 squared displacement, the vibrational modes, and the phonon density of states (DOS).

146 B. Mean-Squared Displacement

147 We first study the particle mean-squared displacements (MSD). We plot the measured
 148 MSD, $\langle \Delta r^2(\Delta t) \rangle$, at different temperatures in Fig. 2. The plateaus at intermediate lag
 149 time scale (Δt) exhibited by the MSDs are signatures of arrested particle dynamics and

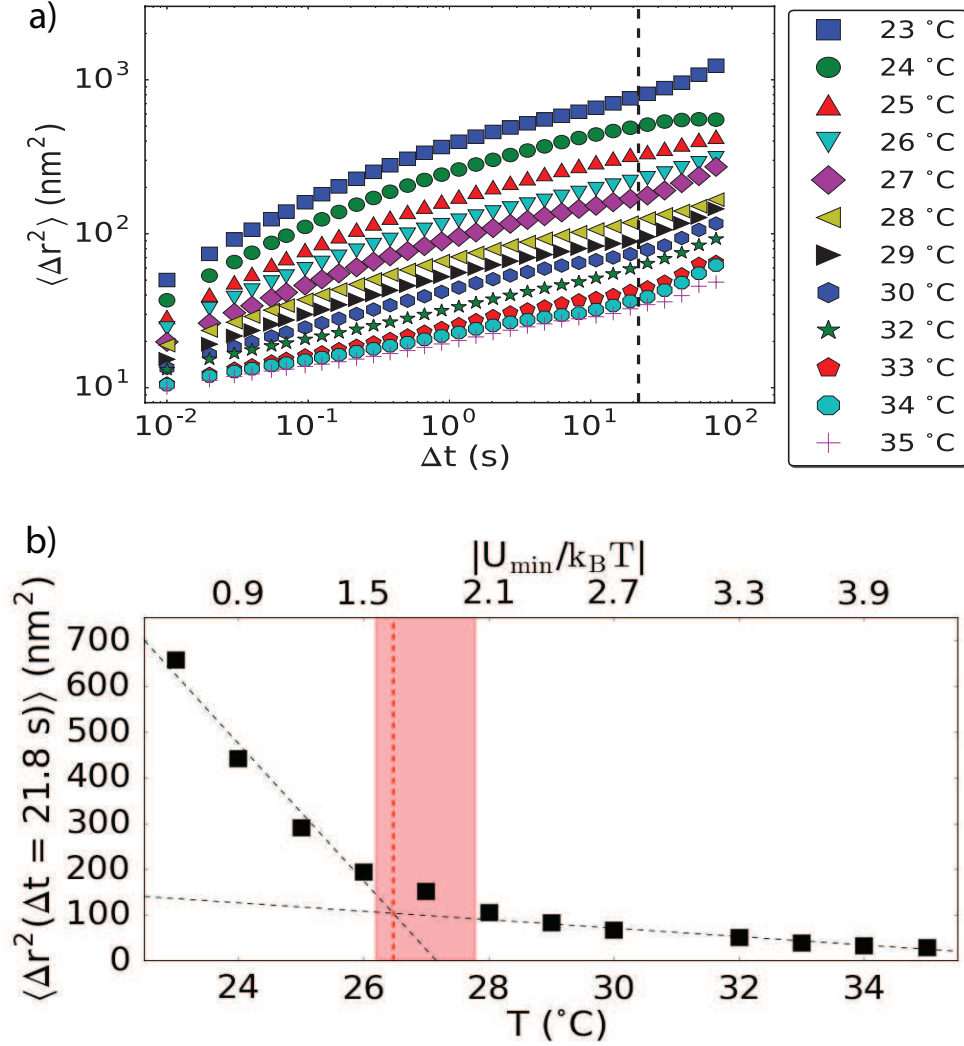


FIG. 2. a) Mean-squared displacement, $\langle \Delta r^2(\Delta t) \rangle$, measured at different temperatures. Dashed line represents lag time $\Delta t = 21.8$ seconds. b) Measured $\langle \Delta r^2(\Delta t) \rangle$ at $\Delta t = 21.8$ seconds as a function of temperature. This behavior is similar for all lag times between 0.1 s and 100 s. The top horizontal-axis indicates the attraction strength $|U_{\min}(T) = k_B T|$ measured in dilute particle suspensions at the temperatures indicated on the bottom horizontal-axis [48]. The black dash lines are linear fitting of data measured at low and high temperatures, corresponding to the repulsive and attractive glasses, respectively. The red dashed line represents the intersection of the two fits. The shaded red region represents the range of temperatures/attraction strengths at which the repulsive-to-attractive glass cross-over could reasonable occur. Error bars are smaller than the size of the symbols.

150 are observed for all temperatures. Notice also, the values of the measured MSDs decrease

151 monotonically with increasing temperature at all lag times. To better demonstrate this
 152 dependency on temperature, we pick out the MSD values at a specific lag time, $\Delta t = 21.8$
 153 seconds, marked by the dash line in Fig. 2(a), and we plot them as a function of temperature,
 154 as shown in Fig. 2(b). These MSD data as a function of temperature clearly show two linear
 155 regions with different slopes in Fig. 2(b). The MSD value decreases at a fast rate when the
 156 temperature is below 26°C , and then saturates above 28°C . Variation in the region between
 157 the two temperatures suggests the existence of a cross-over transition from repulsive to
 158 attractive glass.

159 We estimate the interparticle potentials from experimentally determined pair correlation
 160 functions measured in the dilute concentration regime [48] using liquid structure theory
 161 [65, 66]. Following previous work with this system class [11, 15, 67], we utilize the interaction
 162 potential estimate in the dilute regime as a surrogate for the (unmeasured) potential in the
 163 dense regime. Thus, herein we report the potential measured in dilute regime (which is
 164 unambiguously measured). Thus, in Fig. 2(b) we also provide the measured attraction
 165 strength, *i.e.*, the depth of the attractive potential $|U_{min}|$, on the upper horizontal axis.
 166 Using the attraction strength variation with temperature, the cross-over transition from
 167 repulsive to attractive glass is estimated to be between $1.5k_B T$ and $2k_B T$.

168 Lastly, we note that MSD values at the shorter time scales (less than $\Delta t \sim 10$ seconds)
 169 reflect the free volume size available to the “caged” particle. Thus, decreasing MSD in
 170 this regime indicates shrinking free volumes. In a near-jammed packing with only repulsive
 171 interactions, the free volume is determined by the local packing condition [68]. In our
 172 experiments, interestingly, the reduction in cage size is due solely to the emerging attractive
 173 force. The attraction between contacting particles hinders particle motion, and an attraction
 174 strength of $2 k_B T$ seems to be sufficient to saturate the available volume to particles. While
 175 the transition is comparatively sharp, we definitely do not observe a discontinuous jump in
 176 the MSDs as a function of attraction strength, as was found in the Debye-Waller factors
 177 calculated by MCT [17].

178 C. Vibrational Phonon Behavior

179 To further explore the transition from the repulsive glass state to the attractive glass
 180 state, we calculated the vibrational phonon modes of these colloidal glass samples with

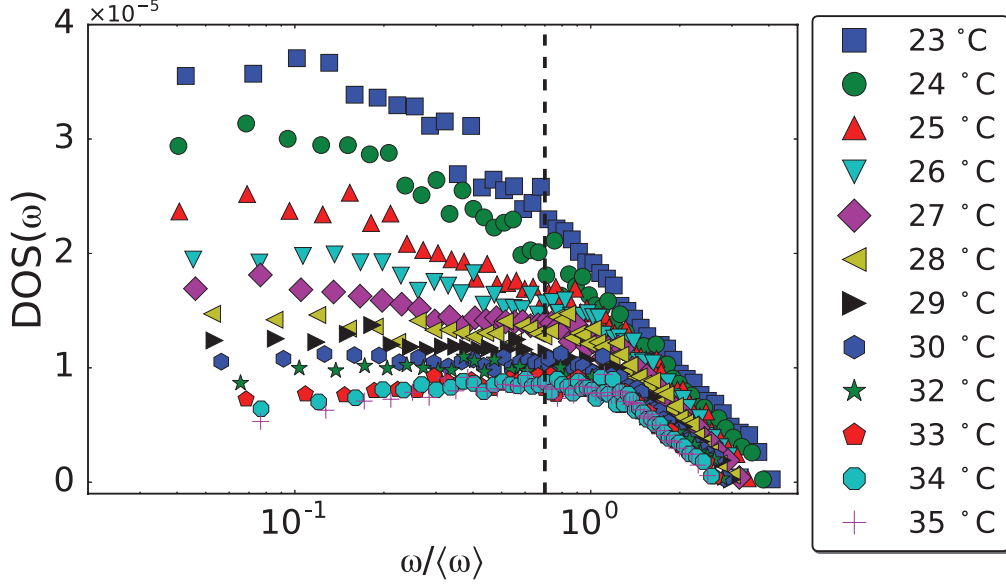


FIG. 3. Vibrational Density of States, $DOS(\omega)$, versus scaled phonon frequency, $\omega / \langle \omega \rangle$, in semi-log plot. Dashed line represents $\omega / \langle \omega \rangle = 0.7$.

181 varying attractive interaction strength between constituents. The resulting distribution of
 182 the $DOS(\omega)$ varies as the strength of interparticle attraction increases (see Figure 3). Specif-
 183 ically, we observe that the $DOS(\omega)$ of the low frequency modes ($\omega / \langle \omega \rangle < 0.7$) decreases as
 184 the strength of the attraction grows. This effect is clearly observed when the $DOS(\omega)$ is
 185 plotted on a log-scale as a function of the phonon frequency scaled by the mean frequency of
 186 each sample, $\omega / \langle \omega \rangle$ (Fig. 3). Qualitatively, the value of $DOS(\omega)$ at low frequencies decreases
 187 monotonically with increasing temperature/attraction strength. To quantify this effect, we
 188 calculated the average $DOS(\omega)$, $\langle DOS(\omega) \rangle$, for modes with $\omega / \langle \omega \rangle < 0.7$ (Figure 4).

189 Using these definitions for the mode ranges, we observe trends that are similar to that
 190 found for the MSD. We find that $\langle DOS(\omega / \langle \omega \rangle < 0.7) \rangle$ decreases monotonically in the low
 191 temperature (low attraction) regime and plateaus at strong attraction strength. Specifically,
 192 we observe that $\langle DOS(\omega / \langle \omega \rangle < 0.7) \rangle$ plateaus at attraction strengths greater than $2k_B T$.
 193 This provides further evidence of a cross-over transition between states of the glass that
 194 occurs when the interparticle attraction strength is approximately $2k_B T$.

195 By contrast, the mean and median phonon frequencies of each sample increased mono-
 196 tonically and smoothly with temperature (Figure 5). No evidence of a cross-over transition
 197 is apparent for these parameters. Again, this continuous increase in the mean and median

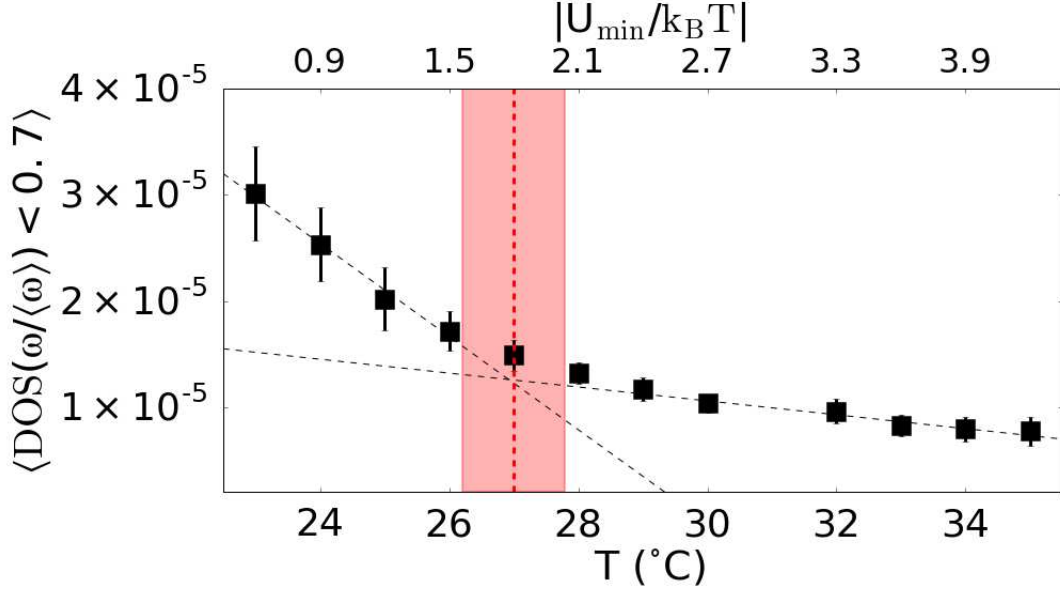


FIG. 4. Average $DOS(\omega)$ for $\omega/\langle\omega\rangle < 0.7$, $\langle DOS(\omega/\langle\omega\rangle < 0.7) \rangle$, for all temperatures, T . The top horizontal-axis indicates the attraction strength $|U_{min}(T) = kBT|$ measured in dilute particle suspensions at the temperatures indicated on the bottom horizontal-axis [48]. Black dashed lines are linear fits to the two regimes (monotonic decrease and plateau), corresponding to the two glass states (repulsive and attractive). The red dashed line represents the intersection of the two fits. The shaded red region represents the range of temperatures/attraction strengths at which the repulsive-to-attractive glass cross-over could reasonably occur.

198 frequencies is consistent with the fact that the interparticle attraction strength increases
 199 linearly with temperature. We expect that with increasing attraction strength, the effective
 200 spring constants, k , between all pairs of particles increase. Increasing spring constants leads
 201 to increasing frequencies since $\omega \propto \sqrt{k}$. The continuous increase of the mean frequencies is
 202 evidence that the strength of the interparticle bonds is continuously increasing. Therefore,
 203 the plateaus observed in the other measured and calculated quantities are not caused by
 204 a saturation in the interparticle bond strength, but are rather due to a saturation of the
 205 dynamical arrest in the system.

206 Lastly, we explored the localized versus extended nature of the low frequency modes.
 207 We computed the so-called mode participation ratio for this purpose. The participation
 208 ratio is defined as $P_R(\omega) = (\sum_{\alpha} e_{\alpha x}^2(\omega) + e_{\alpha y}^2(\omega))^2 / (N_{tot} \sum_{\alpha} e_{\alpha x}^4(\omega) + e_{\alpha y}^4(\omega))$, where $e_{\alpha x}(\omega)$
 209 and $e_{\alpha y}(\omega)$ are the x and y eigenvector components for particle α , respectively. $P_R(\omega) \sim$

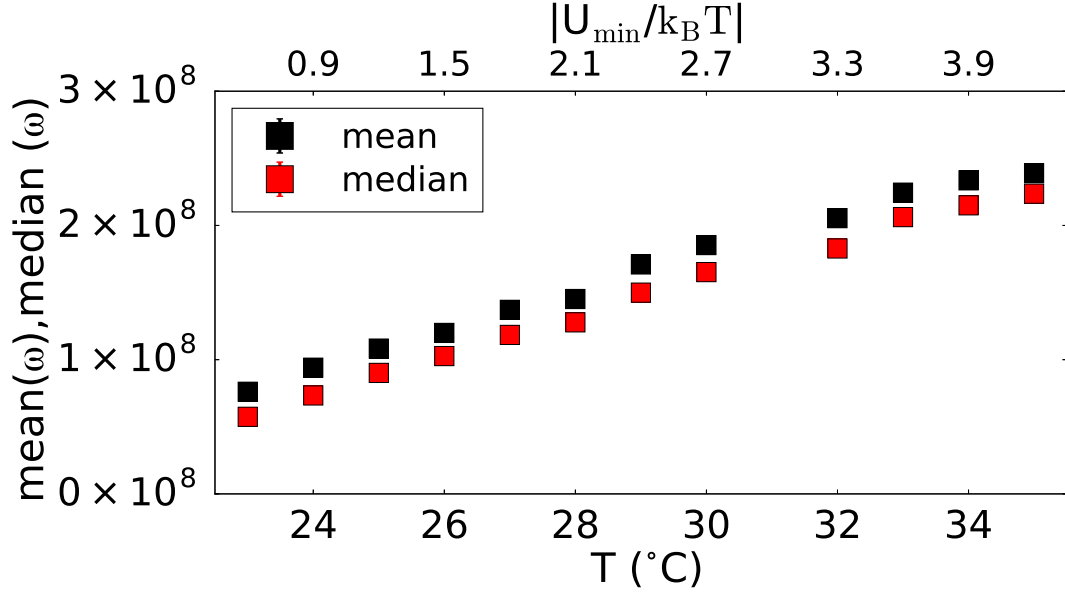


FIG. 5. Mean (black squares) and median (red circles) phonon frequencies vs. temperature. Error bars are smaller than the size of the symbols.

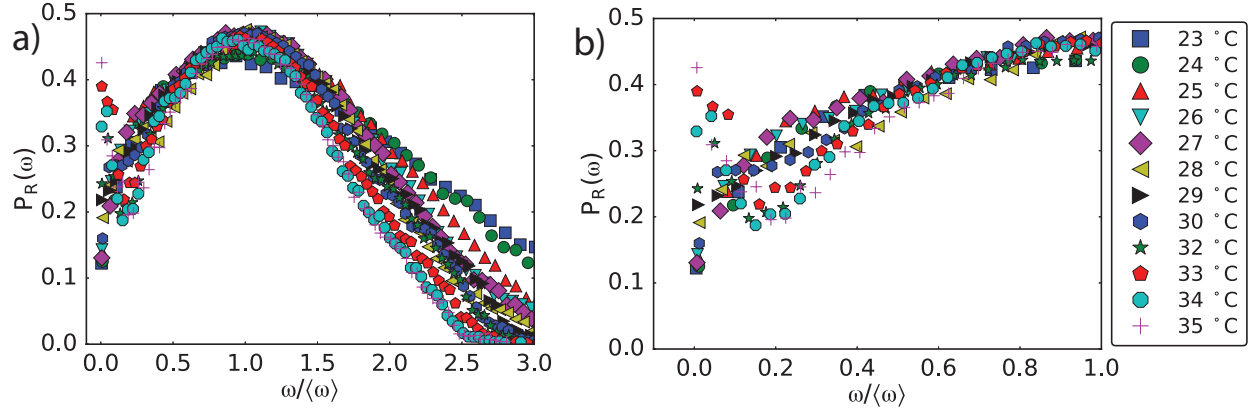


FIG. 6. a) Participation ratio, $P_R(\omega)$, for all temperatures versus scaled frequency, $\omega/\langle\omega\rangle$. b) $P_R(\omega)$ of modes with $\omega/\langle\omega\rangle < 1$.

210 $1/N$ for a localized mode; $P_R(\omega) \sim \mathcal{O}(1)$ for an extended mode. Following convention, we
 211 refer to frequencies with a participation ratio below 0.2 as localized, and frequencies with
 212 participation ratio above 0.2 as extended [34]. At interparticle attractions greater than
 213 $2k_B T$, many more extended modes at low frequencies are observed that are not found in
 214 samples with weaker interparticle attractions (Figure 6).

215 Representative low frequency modes of a repulsive glass and an attractive glass are pre-

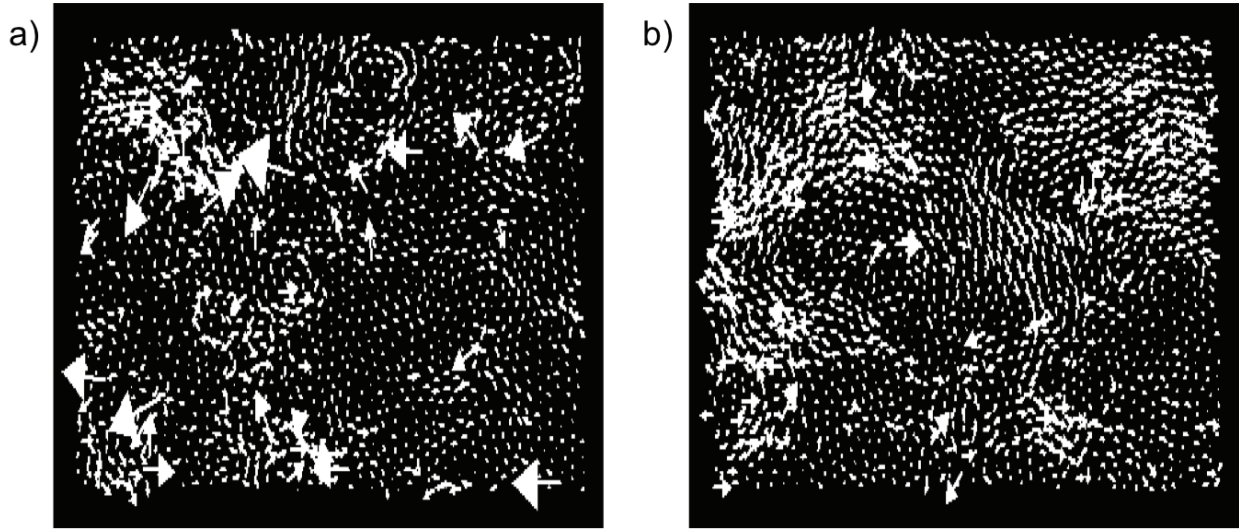


FIG. 7. a) and b) Vector displacement plots of representative low frequency modes in a repulsive glass ($T = 23$ °C, $|U_{min}| = 0.5k_B T$) and an attractive glass ($T = 35$ °C, $|U_{min}| = 4.2k_B T$), respectively.

216 sented in Fig. 7(a) and (b), respectively. These representative modes help visualize the
 217 effect that in repulsive glasses the modes at low frequencies are quasi-localized, whereas
 218 in attractive glasses extended collective motion is found throughout the sample. The low
 219 frequency behavior of the repulsive glasses studied here are consistent with those previously
 220 studied [27, 33, 34, 37–41], specifically that the presence of quasi-localized modes is found.
 221 The extended modes observed here in the low frequency modes of attractive glasses is likely
 222 due to the strong interparticle bonds in attractive glasses. As one particle moves, it pulls its
 223 neighbors with it, who in turn pull their neighbors. This same reasoning can be used to ac-
 224 count for the larger size of cooperative rearrangement regions (CRRs) observed in attractive
 225 glasses compared to CRRs observed in repulsive glasses [15].

226 To quantify the presence of these extended low frequency modes in attractive glasses, we
 227 examined the lowest 100 modes, and we defined modes that have a participation ratio larger
 228 than 0.2 as extended. By measuring the number (within the lowest 100 modes) of modes
 229 that are extended (Figure 8), we again see the same trend as observed in all of our other
 230 data: the number of extended modes plateaus at attraction strengths above $2k_B T$. Thus,
 231 another quantity associated with the phonons exhibits a cross-over trend that saturates
 232 when the attraction strength is larger than $2k_B T$. Again, this saturation effect appears to
 233 signify the transition from the repulsive glass state to the attractive glass state.

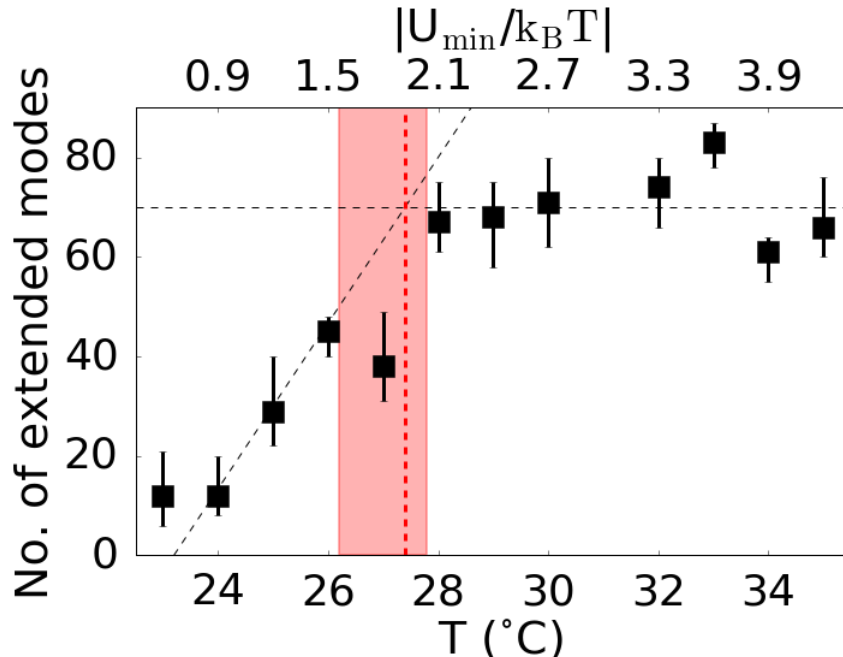


FIG. 8. Number of extended modes ($P_R(\omega) > 0.2$) of the lowest 100 modes. The top horizontal-axis indicates the attraction strength $|U_{min}(T) = k_B T|$ measured in dilute particle suspensions at the temperatures indicated on the bottom horizontal-axis [48]. Black dashed lines are linear fits to the two regimes (monotonic decrease and plateau), corresponding to the two glass states (repulsive and attractive). The red dashed line represents the intersection of the two fits. The shaded red region represents the range of temperatures/attraction strengths at which the repulsive-to-attractive glass cross-over could reasonable occur.

234 IV. CONCLUSION

235 In summary, we experimentally studied the vibrational phonons of 2D colloidal glasses
 236 with increasing attraction strength, and presented evidence that the transition within glassy
 237 colloids occurs from a repulsive glass state to an attractive glass state. From the data, it
 238 appears that the cross-over interparticle attraction strength is $2k_B T$. This transition is sig-
 239 nified by changes in the distribution of the $DOS(\omega)$, as well in the saturation of the particle
 240 dynamics. We observe that repulsive glasses have an excess of low frequency modes com-
 241 pared to attractive glasses. Furthermore, the motion of a majority of the lowest frequency
 242 modes in attractive glasses is spatially extended, wherein in repulsive glasses the motion
 243 at low frequencies is quasi-localized. We also observed that particle dynamics decreased

244 monotonically with increasing attraction strength, but that the particle dynamics are sat-
245 urated for attraction strengths larger than $2k_B T$, signifying the system is reaching a point
246 of maximal arrest. The quantities measured herein did not display a discontinuous jump
247 at the transition point like those calculated from MCT, but they did display a noticeable
248 change in behavior at the transition point.

249 Future work should investigate if the glass re-entrance phenomenon observed in 3D exper-
250 iments [10–13] is also present in 2D samples. This phenomenon is found when the attraction
251 strength between particles increases, and the system transitions from the repulsive glass
252 state to the fluid state. As interparticle attraction strength increases further, the system
253 undergoes a second transition from the fluid state to the attractive glass state. To date,
254 re-entrance has not been observed in 2D. Exploring the properties we have discussed above
255 near re-entrance in 2D would contribute to the larger picture of studying the role of dimen-
256 sionality in the state diagram of glasses with attractive interparticle interactions, and would
257 provide further insight into the glass transition. Also, the variation in the average value
258 of the vibrational density of states at low frequencies, *i.e.*, as observed in the transition
259 from repulsive to attractive glasses, has not to our knowledge been considered theoretically.
260 Future theoretical and simulation work on this problem may be useful for clarifying the
261 underlying mechanisms associated with these observations about phonons in glasses.

262 ACKNOWLEDGMENTS

263 We thank Wei-Shao Wei and Kevin B. Aptowicz for helpful discussions, and M.D.G, X.M,
264 Z.S.D, T.S, and A.G.Y gratefully acknowledge financial support from the National Science
265 Foundation through Grant No. DMR12-05463, the Penn MRSEC Grant No. DMR11-
266 20901 and its optical microscopy SEF, and NASA Grant No. NNX08AO0G. P.H. gratefully
267 acknowledges financial support from the National Science Foundation through Grant No.
268 RUI-1306990.

269 [1] F. Sciortino, Nat Mater **1**, 145 (2002).

270 [2] K. A. Dawson, Current Opinion in Colloid & Interface Science **7**, 218 (2002).

271 [3] G. Foffi, C. De Michele, F. Sciortino, and P. Tartaglia, Phys. Rev. Lett. **94**, 078301 (2005).

- 272 [4] W. R. Hall, and P. G. Wolynes, J. Phys. Chem. B **112**, 301 (2008).
- 273 [5] L. Berthier and G. Tarjus, Phys. Rev. Lett. **103**, 170601 (2009).
- 274 [6] J. Bergenholtz and M. Fuchs, Phys. Rev. E **59**, 5706 (1999).
- 275 [7] A.K. Atmuri, G.A. Peklaris, S. Kishore, S.R. Bhatia, Soft Matter **8**, 8965 (2012).
- 276 [8] D. Marzi, B. Capone, J. Marakis, M.C. Merola, D. Truzzolillo, L. Cipelletti, F. Moingeon,
277 M. Gauthier, D. Vlassopoulos, C.N. Likos, and M. Camargo, Soft Matter **11**, 8296 (2015).
- 278 [9] E. Zaccarelli and W. C. K. Poon, Proc. Natl. Acad. Sci. USA **106**, 15203 (2009).
- 279 [10] K. N. Pham, S. U. Egelhaaf, P. N. Pusey, and W. C. K. Poon, Phys. Rev. E **69**, 011503 (2004).
- 280 [11] L. J. Kaufman and D. A. Weitz, J. Chem. Phys. **125**, 074716, 2006.
- 281 [12] A. Latka, Y. Han, A. M. Alsayed, A. B. Schofield, A. G. Yodh, and P. Habdas, Europhys.
282 Lett. **86**, 58001 (2009).
- 283 [13] N. B. Simeonova, R. P. A. Dullens, D. G. A. L. Aarts, V. W. A. de Villeneuve, H. N. W.
284 Lekkerkerker, and W. K. Kegel, Phys. Rev. E **73**, 041401 (2006).
- 285 [14] C. K. Mishra, A. Rangarajan, and R. Ganapathy, Phys. Rev. Lett. **110**, 188301 (2013).
- 286 [15] Z. Zhang, P. J. Yunker, P. Habdas, and A. G. Yodh, Phys. Rev. Lett. **107**, 208303 (2011).
- 287 [16] L. Fabbian, W. Götze, F. Sciortino, P. Tartaglia, and F. Thiery, Phys. Rev. E **59**, R1347
288 (1999).
- 289 [17] F. Sciortino and P. Tartaglia, Advances in Physics **54**, 471 (2005).
- 290 [18] K. Dawson, G. Foffi, M. Fuchs, W. Götze, F. Sciortino, M. Sperl, P. Tartaglia, Th. Voigtmann,
291 and E. Zaccarelli, Phys. Rev. E **63**, 011401 (2000).
- 292 [19] T. Eckert and E. Bartsch, Phys. Rev. Lett. **89**, 125701 (2002).
- 293 [20] E. Zaccarelli, G. Foffi, K. A. Dawson, S. V. Buldyrev, F. Sciortino, and P. Tartaglia, Phys.
294 Rev. E **66**, 041402 (2002).
- 295 [21] A. M. Puertas, M. Fuchs, and M. E. Cates, Phys. Rev. Lett. **88**, 098301 (2002).
- 296 [22] M. A. Lohr, T. Still, R. Ganti, M. D. Gratale, Z. S. Davidson, K. B. Aptowicz, C. P. Goodrich,
297 D. M. Sussman, and A. G. Yodh, Phys. Rev. E **90**, 062305 (2014).
- 298 [23] N. Koumakis and G. Petekidis, Soft Matter **7**, 2456 (2011).
- 299 [24] C. L. Klix, F. Ebert, F. Weysser, M. Fuchs, G. Maret, and P. Keim, Phys. Rev. Lett. **109**,
300 178301 (2012).
- 301 [25] C. L. Klix, G. Maret, and P. Keim, Phys. Rev. X **5**, 041033 (2015).
- 302 [26] W. A. Phillips, editor, Springer, 1st edition, (1981).

- 303 [27] K. Chen, W. G. Ellenbroek, Z. Zhang, D. T. N. Chen, P. J. Yunker, S. Henkes, C. Brito,
304 O. Dauchot, W. van Saarloos, A. J. Liu, and A. G. Yodh, Phys. Rev. Lett. **105**, 025501
305 (2010).
- 306 [28] A. Ghosh, V. K. Chikkadi, P. Schall, J. Kurchan, and D. Bonn, Phys. Rev. Lett. **104**, 248305
307 (2010).
- 308 [29] S. Franzà, G. Parisi, P. Urbani, and F. Zamponi, Proc. Nat. Acad. Soc. **112**, 14539 (2015).
- 309 [30] V. Lubchenko and P.G. Wolynes, PNAS **100**, 1515 (2003).
- 310 [31] E. Stavrou, C. Tsiantos, R.D. Tsofouridou, S. Kriptou, A.G. Kontos, C. Raptis, B. Capoen,
311 M. Bouazaoui, S. Turrell, and S. Khatir, J. Phys. Condens. Matter **22**, 195103 (2010).
- 312 [32] H. Kobayashi and H. Takahashi, J. Non-Crystal. Solids **427**, 34 (2015).
- 313 [33] N. Xu, V. Vitelli, A. J. Liu, and S. R. Nagel, Europhys. Lett. **90**, 56001 (2010).
- 314 [34] K. Chen, M. L. Manning, P. J. Yunker, W. G. Ellenbroek, Z. Zhang, A. J. Liu, and A. G.
315 Yodh, Phys. Rev. Lett. **107**, 108301 (2011).
- 316 [35] A. Ghosh, V. Chikkadi, P. Schall, and D. Bonn, Phys. Rev. Lett. **107**, 188303 (2011).
- 317 [36] M. L. Manning and A. J. Liu, Phys. Rev. Lett. **107**, 108302 (2011).
- 318 [37] A. Widmer-Cooper, H. Perry, P. Harrowell, and D. R. Reichman, J. Chem. Phys. **131**, 194508
319 (2009).
- 320 [38] A. Widmer-Cooper, H. Perry, P. Harrowell, and D. R. Reichman, Nat. Phys. **4**, 711 (2008).
- 321 [39] A. Tanguy, B. Mantsi, and M. Tsamados, Europhys. Lett. **90**, 16004 (2010).
- 322 [40] C. Brito and M. Wyart, J. of Stat. Mech. **8**, L08003 (2007).
- 323 [41] K. Sun, A. Souslov, X. Mao, and T. C. Lubensky, Proc. Natl. Acad. Sci. USA **109**, 12369
324 (2012).
- 325 [42] R. Zargar, J. Russo, P. Schall, H. Tanaka and D. Bonn, Europhys. Lett. **108**, 38002 (2014).
- 326 [43] N. L. Green, D. Kaya, C. E. Maloney, and M. F. Islam, Phys. Rev. E **83**, 051404 (2011).
- 327 [44] P. Tan, N. Xu, A. B. Schofield, and L. Xu, Phys. Rev. Lett. **108**, 095501 (2012).
- 328 [45] X. Wang, W. Zheng, L. Wang, and N. Xu, Phys. Rev. Lett. **114**, 035502 (2015).
- 329 [46] M. Wyart, Europhys. Lett. **89**, 64001 (2010).
- 330 [47] J. R. Savage and A. D. Dinsmore, Phys. Rev. Lett. **102** 198302, (2009).
- 331 [48] M. D. Gratale, T. Still, C. Matyas, Z. S. Davidson, S. Lobel, P. J. Collings, and A. G. Yodh,
332 Phys. Rev. E **93**, 050601 (2016).
- 333 [49] R. Yamamoto and A. Onuki, Phys. Rev. E **58**, 3515 (1998).

334 [50] D. N. Perera and P. Harrowell, *J. Chem. Phys.* **111**, 5441 (1999).

335 [51] P. Yunker, Z. Zhang, and A. G. Yodh, *Phys. Rev. Lett.* **104**, 015701 (2010).

336 [52] S. J. Gerbode, D. C. Ong, C. M. Liddell, and I. Cohen, *Phys. Rev. E* **82**, 041404 (2010).

337 [53] J. C. Crocker and D. G. Grier, *J. of Colloid and Interface Sci.* **179**, 298 (1996).

338 [54] D. Kaya, N. Green, C. Maloney, and M. Islam, *Science*, **329**, 656 (2010).

339 [55] S. Henkes, C. Brito, and O. Dauchot, *Soft Matter*, **8**, 6092 (2012).

340 [56] M. Schindler and A.C. Maggs, *Eur. Phys. J. E* **34**, 115 (2011).

341 [57] A. Ghosh, R. Mari, V. K. Chikkadi, P. Schall, A. C. Maggs, D. Bonn, *Physica A* **390**, 3061
342 (2011).

343 [58] C. A. Lemarchand, A. C. Maggs and M. Schindler, *Europhys Lett.* **97**, 48007 (2012).

344 [59] A. C. Maggs and M. Schindler, *Europhys Lett.* **109**, 48005 (2015).

345 [60] A. Hasan and C. E. Maloney, *Phys. Rev. E* **90**, 062309 (2014).

346 [61] K. Chen, T. Still, S. Schoenholz, K.B. Aptowicz, M. Schindler, A.C. Maggs, A.J. Liu, and
347 A.G. Yodh, *Phys. Rev. E* **88**, 022315 (2013).

348 [62] T. Still, C.P. Goodrich, K. Chen, P.J. Yunker, S. Schoenholz, A.J. Liu, and A.G. Yodh, *Phys.*
349 *Rev. E* **89**, 012301 (2014).

350 [63] J. D. Weeks, D. Chandler, and H. C. Andersen, *J. Chem. Phys.* **54**, 5237 (1971).

351 [64] J. Taffs, A. Malins, S. R. Williams, and C. P. J. Royall, *J. Chem. Phys.* **133**, 244901 (2010).

352 [65] Y. L. Han and D. G. Grier, *Phys. Rev. Lett.* **91**, 038302 (2003)

353 [66] J. Baumgartl and C. Bechinger, *Europhys. Lett.* **71**, 487 (2005).

354 [67] L. Parolini, A. D. Law, A. Maestro, D. M. A. Buzza, and P. Cicuta, *J. Phys.: Condens. Matter*
355 **27**, 194119 (2015).

356 [68] E. R. Weeks, J. C. Crocker, A. C. Levitt, A. Schofield, and D. A. Weitz, *Science* **287**, 627
357 (2000).